Production of Hydrogen and Carbon Nanotubes from Catalytic Decomposition of Methane over Ni:Cu/Alumina Modified Supported Catalysts

Tajammul Hussain,* Mohammed Mazhar, Sarwat Iqbal, Sheraz Gul, Muzammil Hussain, and Faical Larachi†

*Department of Chemistry, Quaid-i-Azam University, Islamabad, Pakistan. *E-mail: dr_tajammul@yahoo.ca*
†Department of Chemical Engineering, University of Laval, Quebec, Sainte-Foy, G1K 7P4, Canada
Received January 18, 2007

Hydrogen gas and carbon nanotubes along with nanocarbon were produced from commercial natural gas using fixed bed catalyst reactor system. The maximum amount of carbon (491 g/g of catalyst) formation was achieved on 25% Ni, 3% Cu supported catalyst without formation of CO/CO_2. Pure carbon nanotubes with length of 308 nm having balloon and horn type shapes were also formed at 673 K. Three sets of catalysts were prepared by varying the concentration of Ni in the first set, Cu concentration in the second set and doping with K in the third set to investigate the effect on stabilization of the catalyst and production of carbon nanotubes and hydrogen by copper and potassium doping. Particle size analysis revealed that most of the catalyst particles are in the range of 20-35 nm. All the catalysts were characterized using powder XRD, SEM/EDX, TPR, CHN, BET and CO-chemisorption. These studies indicate that surface geometry is modified electronically with the formation of different Ni, Cu and K phases, consequently, increasing the surface reactivity of the catalyst and in turn the Carbon nanotubes/H_2 production. The addition of Cu and K enhances the catalyst dispersion with the increase in Ni loadings and maximum dispersion is achieved on 25% Ni: 3% Cu/Al catalyst. Clearly, the effect of particle size coupled with specific surface geometry on the production of hydrogen gas and carbon nanotubes prevails. Addition of K increases the catalyst stability with decrease in carbon formation, due to its interaction with Cu and Ni, masking Ni and Ni:Cu active sites.

Key Words : CH_4 decomposition, Ni:Cu/Al catalysts, Carbon nanotubes, Hydrogen

Introduction

Catalytic decomposition of methane into hydrogen and carbon is of immense present day interest as an alternate source for production of hydrogen to use it as a clean source of energy. The catalyst used for this purpose is supported nickel. The process of catalytic decomposition of natural gas encountered several problems that include simultaneous production of CO and CO_2, catalyst deactivation and particles size effect on the carbon production.[1-13] It is also reported in the literature that typical 40% Ni/SiO_2 catalyst yields carbon as high as 491 gC/gNi at 773 K.[14] Another study indicates that the carbon yield with 75%Ni-15% Cu/aluimna supported catalyst prepared by co-precipitation method gives a carbon yield of 700 g/gNi at 898 K.[11] The purification (chemical or mechanical) of carbon from the catalyst is also quite cumbersome.

To improve the overall efficiency of the process and yield of carbon in the pure form, synthesis of the catalyst system with controlled particle size and surface morphologies todate becomes one of the important areas of R & D in catalyst development.[15] Various techniques like sole-gel, metal-organic vapor deposition and thermal decomposition used to address the problems suffered a set back due to agglomeration of material during calcinations,[16-20] which consequently effects the carbon and hydrogen production and results in very fast catalyst deactivation.

It has also been reported in the literature that doping Ni/alumina and Ni/silica catalysts with alkali and alkaline earth metal oxides enhances the catalyst stability and reactivity[21-29] because of the modification of surface geometry electronically.[30-33] Again, the agglomeration of particles leads to the deactivation of catalyst resulting in less carbon formation.

In the present study, carbon nanotubes and hydrogen were produced at low temperature (673 K) as compared to that reported in literature.[34-48] We described a new catalyst preparation method that enabled us to prepare a catalyst system with controlled particle size and good metal dispersion which resulted in the production of pure carbon nanotubes without CO/CO_2 production at relatively mild temperature. This controlled particle size catalyst when doped with potassium has a significant effect on the catalyst stability and reactivity.

Experimental

Catalyst Characterization. X-ray diffraction patterns were determined by a Rigaku RINT 2500 V diffractometer using Cu-Kα radiation at room temperature operated at 40 kV and 100 A. The mean crystallite sizes of the fresh and spent catalyst samples were calculated using the Scherer equation, where the particle factor was taken as 0.9.[39]

SEM images and backscattering electron images of the catalysts were determined using a Hitachi FE-SEM S-800 (field emission gun scanning electron microscopy).

The N_2 adsorption-desorption isotherms were obtained using a Nova 4200e (Quantachrome) system operated at 77

K. Before these measurements, all the samples were degassed by vacuum at 573 K for 5 hours. The BET surface area was calculated from the multipoint BET analysis of nitrogen adsorption isotherm.

The particle size analyses were performed using sorptometer KELVIN 1042, supplied by COSTECH instruments.

The temperature programmed reduction (TPR) was performed in a conventional set up equipped with a thermal conductivity detector (TCD). In a typical run, 50 mg catalyst/catalysts samples were used and heated to 673 K (10 K/min) under Nitrogen flow (40 mls/min) and kept at this temperature for 0.5 hours to remove the adsorbed species on the fresh samples. On the spent samples no treatment was performed. After cooling down to room temperature the reduction gas (20 vol% H_2/N_2) was introduced (40 mls/min). The temperature was then programmed to rise from room temperature to 1073 K at the ramp of 10 K/min. CHN analyses were performed on the fresh and spent catalysts using EA1112 (Thermo Electron) equipment.

Catalysts Preparation. Aluminum acetate basic was soaked in 50 mL of distilled water. $Ni(NO_3)_2{\cdot}6H_2O$ and $Cu(NO_3)_2{\cdot}2H_2O$ were added to the mixture with constant stirring. This slurry was kept soaked at room temperature overnight. The water was evaporated at 120 °C and kept at this temperature for 12 hours. The dried powder was calcined at 923 K for six hours. Three sets of catalyst samples were prepared, one keeping the copper concentration constant and varying the Ni concentration, the other set in which copper concentration was varied keeping nickel concentration constant and the third set of samples was prepared in which nickel and copper concentration were kept constant and potassium concentration was varied. Samples of first set were designated as Ni:Cu/Al: 10:3, Ni:Cu/Al: 15:3, Ni:Cu/Al: 25:3, the other set as Ni:Cu/Al: 25:10, Ni/Al: 25:75 and the third set as Ni:Cu:K/Al: 25:3:0.5, Ni:Cu:K/Al: 25:3:1.0, Ni:Cu:K/Al: 25:3:1.5. Potassium doped samples were also prepared using the same procedure described above. The catalyst preparation details and amount of respective salts used with the support are presented in Table 1(a-d). In all the preparations impregnation of metal oxides is based on the weight percentage of metal nitrates.

Catalyst Testing. Methane decomposition over all the prepared catalysts was carried out in the conventional gas flow system. The catalyst loading of 0.5 g was put at the bottom of the SS reactor with quartz wool at both ends, the alumina support was used to hold the catalyst. The sample was reduced in hydrogen flow (100 mls/min) for 8-hours at 450 °C. The temperature was then lowered to 400 °C and methane decomposition was initiated by the contact of stream of methane ($P_{(CH_4)}$ = 100 kP_a, flow rate 60 mls/min)

Table 1. EDX and BET analysis of the prepared catalyst samples

(a)

Catalyst Designation	Wt. of Ni salt used (g)/(mmol)	Wt. of Cu salt used (g)/(mmol)	Wt. of K salt used (g)/(mmol)	Wt. of support (g)/(mmol)
10%Ni:3%Cu/Al	2.4775/8.52	0.5703/2.36	–	26.1303/161.22
15%Ni:3%Cu/Al	3.7163/12.78	0.5703/2.36	–	24.6286/151.95
25%Ni:3%Cu/Al	6.1938/21.30	0.5703/2.36	–	21.6251/133.42
25%Ni:10%Cu/Al	6.1938/21.30	1.9010/7.87	–	19.5226/120.45
25%Ni/75%Al	6.1938/21.30	–	–	22.5261/138.98
25%Ni:3%Cu:0.5%K/Al	6.1938/21.30	0.5703/2.36	0.0646/0.64	21.4749/132.50
25%Ni:3%Cu:1.0%K/Al	6.1938/21.30	0.5703/2.36	0.1293/1.28	21.3247/131.57
25%Ni:3%Cu:1.5%K/Al	6.1938/21.30	0.5703/2.36	0.1939/1.92	21.1746/130.64

(b) Set No. 1

Catalyst Designation	% Cu	%Ni	Surface area m^2g^{-1}
10%Ni:3%Cu/Al	2.92	9.3	141
15%Ni:3%Cu/Al	2.90	14.1	152
25%Ni:3%Cu/Al	2.96	24.3	196

(c) Set No 2

Catalyst Designation	%Ni	%Cu	Surface area m^2g^{-1}
25%Ni/Al		23.9	112
25%Ni:10%Cu/Al	23.78	8.79	90

(d) Set No. 3

Catalyst Designation	%Ni	%Cu	%K	Surface area m^2g^{-1}
25%Ni:3%Cu:0.5%K/Al	24.7	2.92	0.41	87
25%Ni:3%Cu:1.0%K/Al	23.98	2.90	0.90	78
25%Ni:3%Cu:1.5%K/Al	23.96	2.95	1.34	69

with the catalyst. During methane decomposition, part of stream gases of the catalyst bed was sampled and analyzed by GC. Conversion of methane was evaluated from the amount of hydrogen formed, assuming that the reaction, $CH_4 \rightarrow C + 2H_2$, proceeded selectively. In fact, hydrogen and unreacted CH_4 were confirmed as gaseous products during the reaction.

Table 1. shows the %age composition of all the catalyst samples for Ni, Cu and K and the BET surface area. It can be seen from Table 1(a-c) that atomic %ages of Ni, Cu and K determined after preparation of the catalyst agree well with the theoretical values confirming that the preparation procedure we adopted results in the maximum coating of the Ni, Cu and K on to the support. Consequently, any change in the catalyst activity and selectivity reported in this article is due to surface modification by Cu, K, and particle size rather than the inhomogeneous deposition of Ni, Cu and K on to the support.

Results and Discussions

Catalyst Characterization

Catalyst Characterization Using XRD. Figure 1 shows the XRD patterns of the samples, fresh and spent. All the fresh and spent samples showed a typical face centered cubic structure. This is an indication that carbon nano tubes formation on the spent catalyst does not effect the phase of the material. A consistent decrease in the intensity of metal oxides' peaks is observed with an increase in Nickel loadings in comparison with parent Nickel sample, which reveals modification in the catalyst geometry.

The particle size showed a marked decrease on the spent catalyst, clearly indicating the formation of carbon nano particles (Table 2). The surface morphologies of Cu and K doped samples showed a marked change due to surface modification electronically of the catalyst resulting from addition of K, consequently modifying the textural properties of the catalysts. The addition of K does not appreciably effect the particle size, this gives support to our argument that the addition of K electronically modified the surface geometry, and the particle size effect on K doped sample is suppressed by the electronic modification of surface by K addition, thus the carbon formation on K doped sample is reduced quite substantially.

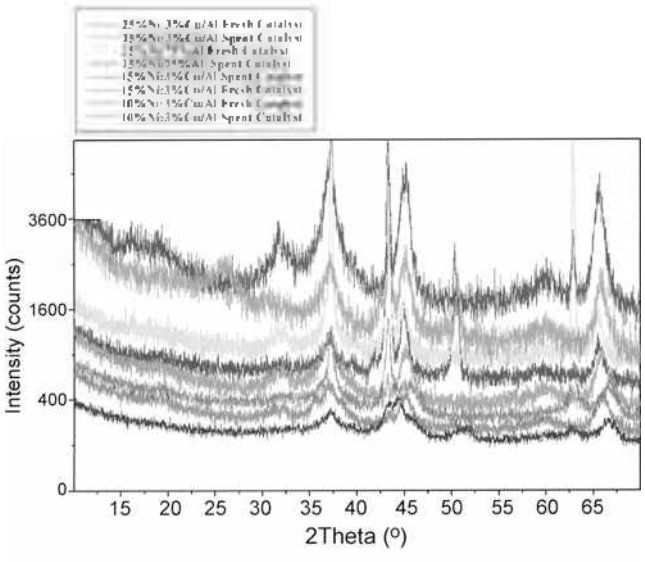

Figure 1. XRD analysis of the prepared catalyst samples.

Table 2. Estimation of crystallite size using XRD data

Catalyst Designation	Fresh (nm)	Spent (nm)
10%Ni:3%Cu/Al	30.2	17.95
15%Ni:3%Cu/Al	34.6	20.02
25%Ni:3%Cu/Al	25.6	13.6
25%Ni:10%Cu/Al	32.98	18.09
25%Ni:3%Cu:1%K/Al	44.66	37.94
25%Ni/Al	29.25	11.54

Table 3 shows the amount of CO adsorbed on the catalyst samples. The amount decreases on the spent catalysts and on K doped samples indicating the surface coverage of catalyst by carbon and potassium. As the Ni concentration increases the amount of CO adsorbed on the fresh catalyst samples increases, an indication of modified surface geometry. This is supported by SEM where carbon formation increases with the increase in Ni concentration.

The surface weighted average particle sizes of the promoted and unpromoted catalysts were roughly estimated from CO-chemisorption to be in the range of 16.00 nm to 30.00 nm on fresh samples indicating good agreement with the values obtained from XRD. The Ni surface areas of all the catalyst samples were calculated using the following equation.

$$D_p\,(\text{nm}) = 1.01/D$$

The dispersion of the catalyst system having 25%Ni: 3%Cu/Al was found to be the maximum as indicated in Tables 3 and 4. This indicates that the modified procedure adopted in the preparation of catalysts gives a high dispersion of Ni on the surface of the catalyst in comparison with the conventional methods used to date.

The coverage of Ni (θ_K), by K, was calculated from the CO adsorption data. CO chemisorption results (Table 3) showed a substantial decrease in Ni coverage on the K doped samples indicating that K addition masked the emission of Ni. We suggest here that due to this modification in the material characteristics, K addition has direct effect on the formation of CNT's/NC and also on the stability of the catalysts during CH_4 decomposition.

The active Ni surface area per gram of catalyst, as estimated using CO-chemisorption and Ni atom area (6.5×10^{-20} m^2 $atom^{-1}$), was 2.6-6.1 m^2 $g\text{-}cat.^{-1}$.

Catalyst Characterization Using Temperature Programmed Reduction (TPR). Figure 2 illustrates the H_2-TPR profile of the catalyst samples (fresh). The figure shows a broad peak around 400 °C representing the characteristic reduction of Ni:Cu. Jenkins *et al.* showed the TPR-H_2 reduction peaks around 360 °C, which they assigned to the characteristic reduction of stiochiometric nickel oxide.[40] In

Table 3. Characterization of catalyst samples using selective CO-chemisorption

Catalyst Designation	Ni crystallite size (nm)	CO-adsorption (μmolg^{-1}) (Fresh)	CO-adsorption (μmolg^{-1}) (Spent)	Ni Coverage (θ_K) (Fresh)	% Ni Dispersion
10%Ni:3%Cu/Al	24.39	98	83	0.33	4.1
15%Ni:3%Cu/Al	20.83	110	90	0.42	4.9
25%Ni:3%Cu/Al	16.39	123	101	0.58	6.1
25%Ni:10%Cu/Al	26.31	112	100	0.49	3.8
25%Ni:3%Cu:1%K/Al	38.46	90	82	0.20	2.6
25%Ni/Al	30.33	80	73	0.10	3.3

Table 4. Estimation of %age Ni dispersion using the particle size calculated from XRD data

Catalyst Designation	%age Ni dispersion Fresh	%age Ni dispersion Spent
10%Ni:3%Cu/Al	3.34	5.63
15%Ni:3%Cu/Al	2.92	5.045
25%Ni:3%Cu/Al	3.94	7.43
25%Ni:10%Cu/Al	3.06	5.58
25%Ni:3%Cu:1%K/Al	2.26	4.63
25%Ni/Al	3.45	3.78

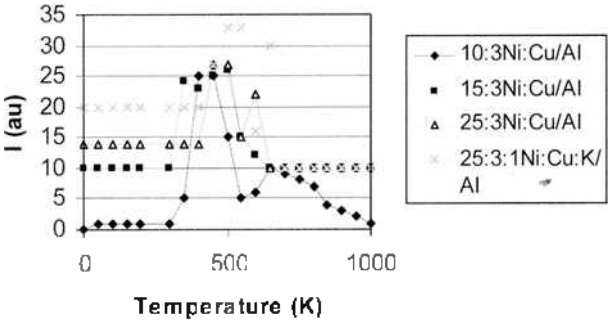

Figure 2. H_2-TPR profile of Ni:Cu/Al & Ni:Cu:K/Al samples.

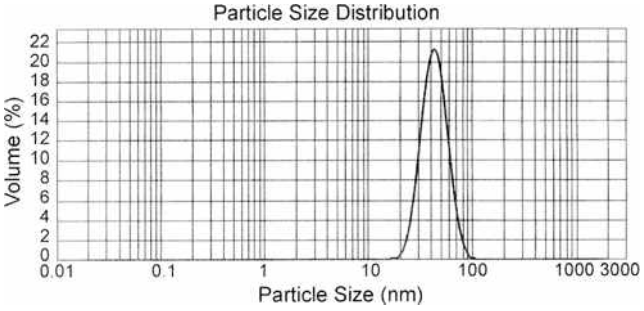

Figure 3. Particle size analysis of 25%Ni:3%Cu/Al sample.

our case the peak is slightly higher, indicating the surface modification and formation of Cu:Ni bimetallic. As the Ni concentration in the sample increases not only the reduction peak is shifted to higher temperature but also it splits into two distinct peaks one indicating the NiO reduction and the other representing the reduction of Ni:Cu bimetallic. For K doped samples the reduction peak shifted to higher temperature, an indication of electronic effect due to addition of K. Although, K doped samples have a different particle size and particle shape, they exhibited similar reduction features with strong hydrogen reduction peaks from 360-500 °C. The procedure we have adopted in the preparation of controlled size particle supports the above observation and we suggest that Al^{3+} is incorporated into the Ni:Cu frame work and inhibits the crystal growth during the CH_4 decomposition reaction. This probably makes the Ni reduction easy. The TPR profile of the systems supports our findings. XRD and TPR data suggest that an appropriate value of 3/1 exists in the Ni/Al ratio which may be the basic reason for the formation of highly dispersed Ni:Cu/Al catalysts. The highest reduction temperatures are observed for 25%Ni:3%Cu/Al catalyst, which also shows that the best dispersion can only be achieved up to 25% Ni concentration. It is concluded that the effect of Ni hydrotalcite affords a substantial effect on the formation of highly dispersed catalyst. On the higher concentration of Ni this structure is lost and this is the reason that the dispersion of catalyst reduces on higher Ni loaded samples. We also propose here that the formation of Ni-Aluminates also contributes to the increase in reduction temperature with the increase in Ni loading and consequently the catalyst dispersion and reactivity of the catalysts. This is supported by XRD data where the Ni-Aluminates are formed on higher loaded Ni catalyst samples than 25% Ni. It must also be noted that the formation of Ni^{+2} is controlled by the incorporation of Al^{3+} during the preparation which controls the dispersion and phase change parameters.

XRD observation of the catalyst samples after the reaction showed not only the change in the angle of diffraction but also an appreciable change in particle size suggesting the formation of nano carbon particles and also the change in surface morphology of the catalysts. This is also supported by the CHN analysis reported in Table 6, where maximum carbon/carbon tubes formation is observed on the 25%Ni:3%Cu/Al sample.

Particle Size and Morphology of the Catalyst Systems. Particle size analysis of our most effective sample is shown in Figure 3. This is good indication of the preparation of controlled particle size catalysts used in the present study.

From the reaction results of methane decomposition, it seems that the initial particle size and morphology of nickel catalysts had an important effect on the catalytic performance. We propose here, based on our XRD results, that on the spent catalysts average particle size decreases in comparison with the fresh sample. This is pointing out the formation of graphitic type of carbon (less reactive carbon).

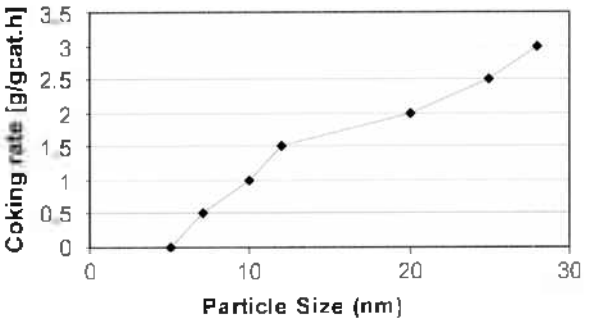

Figure 4. Effect of particle size on the coking threshold. (25%Ni: 3%Cu/Al catalyst).

Rostrup-Nielson,[41] on the basis of theoretical studies, pointed out that the smaller the particle size, closer will be the thermodynamic properties to graphite, which yields a high coking threshold. On the basis of this argument, the effect of Cu becomes more pronounced, which though yields substantial amount of carbon but the presence of Cu prevents the formation of reactive type of carbon and in turn no CO and CO_2 is produced.

The value of the coking threshold during methane decomposition can be extrapolated from the curve shown in Figure 4. The coking threshold is 3.0 on 28 nm Ni crystals, whereas it is about 1.5 on 12 nm Ni crystals. This also supports our argument that the particle size coupled with Cu interaction has a well defined effect on our samples.

Mechanism of Formation of CN Fibers/Tubes. It has been generally accepted that the mechanism of formation of CNF/T includes the adsorption of disintegrated carbon from hydrocarbons *via* catalytic surface reactions, subsequent segregation of surface carbon into layers near the surface, diffusion of carbon through Ni and then precipitation on the rear side of the Ni particle. The process will lead to the formation of CNF/T, as presented in the following equations.

$$CH_4 + 2S = CH_3\text{-}S + H\text{-}S \quad (1)$$

$$CH_3\text{-}S + S = CH_2\text{-}S + H\text{-}S \quad (2)$$

$$CH_2\text{-}S + S = CH\text{-}S + H\text{-}S \quad (3)$$

$$CH\text{-}S + S = C\text{-}S + H\text{-}S \quad (4)$$

$$2H\text{-}S = H_2 + 2S \quad (5)$$

Dissolution/Segregation

$$C\text{-}S = C_{Ni,f} + S \quad (6)$$

Diffusion of carbon through Nickel

$$C_{Ni,f} \rightarrow C_{Ni,r} \quad (7)$$

Precipitation/dissolution of carbon

$$C_{Ni,r} = C_1 \quad (8)$$

Encapsulating carbon formation:

$$nC\text{-}S = S_{encapsulating}$$

where S is the adsorption site; $C_{Ni,f}$ is the carbon dissolved in nickel at the front of the particle, just below the selvage; $C_{Ni,r}$ is the carbon dissolved in nickel at the rear side of the particle (support side); $C_{encapsulating}$ represents the encapsulating carbon formation on the Ni surface, which deactivates the catalysts; and n is the ensemble size.

The yield of CNFs/CNTs depends on the initial coking rate and on the deactivation rate. In principal, high initial coking rates combined with low deactivation rate will result in high yields of CNFs/CNTs. Based on the SEM image presented in Figure 10 and XRD results presented in Figure 11 for K doped samples, it could be concluded that maximum yield of CNFs/CNTs can be obtained on a Ni crystal size of about 28 nm.

However, it could be argued that support may have effects, other than Ni crystal size, on the coking rate and on the deactivation. The effect of support on the formation CNFs/CNTs has been studied widely.[42,43] Most of the studies have focused on the effect of support on the diameter and the distribution of CNFs as well as on their morphology. Colin Park and Mark A. Keane[44] studied Ni as catalyst and Al_2O_3, MgO, SiO_2 and Ta_2O_5 as support materials for the production of CNFs. They found out that the support influenced not only the diameter of CNFs but also the density of CNFs as observed in SEM images, which were used as an index of CNF yield.

In the present study we have found that the preparation procedure of the catalysts we have adopted, gives a very narrow band of particle size, the particle size and the probability of carbon growth is presented in Figure 5 and the maximum growth of CNTs occurred in the range of 25-30 nm particle size which amounts to be 48-50% carbon production as presented in EDAX analysis (Figure 7 and Table 5) and CHN analysis reported in Table 6. The CNTs obtained from Ni nanoparticles with the average diameter of 25-30 nm have length of 318.0 nm (Figure 8). The striking feature of this study is the production of single tube of nano carbon and very pure too. Such CNTs can directly be sued for hydrogen storage without any further treatment. This study will be presented else where.

Based on our SEM findings, the amorphous nature of CNTs is quite evident and is very high. Another important feature is the formation of balloon and horn type CNTs which have considerable large length and diameter. This can be attributed to the presence of copper in the sample which produces sites responsible for the formation of amorphous CNTs. No other form of carbon is formed and it is supported

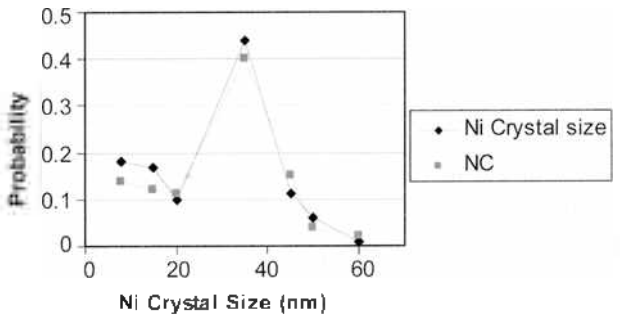

Figure 5. Effect of Particle size on carbon growth (catalyst 25%Ni: 3%Cu/Al).

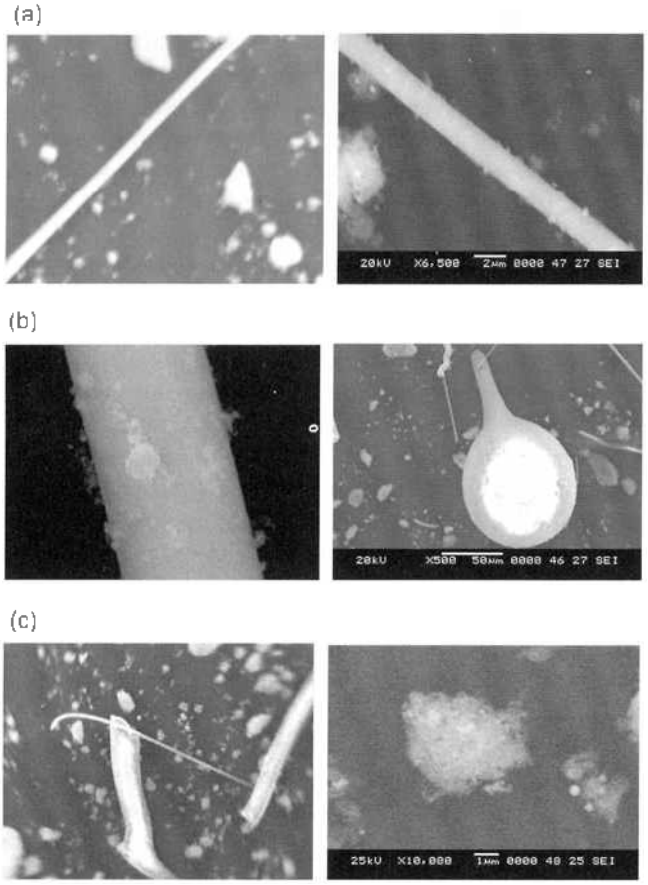

Figure 6. (a) SEM analysis of 10% and 15%Ni:3%Cu/Al catalyst. (b) SEM analysis of 25%Ni:3%Cu/Al catalyst showing pure and balloon type CNTs production. (c) SEM analysis of 25%Ni:3%Cu/Al catalyst showing horn type CNTs and 25%Ni:75% Al catalyst showing formation of nano carbon only.

by XRD results, meaning that rather high purity CNTs are formed. This is partially due to low temperature used for the reaction but mainly due to presence of Cu. The low temperature avoids carbon deposition by gas phase reaction. The results of catalytic studies indicate that no CO and CO_2 are formed, so the hydrogen produced in the present study is rather very pure.

Catalysts Characterization Using SEM. Figure 6(a-g) shows the SEM images of carbon nanotubes formed on different Ni loading samples after methane decomposition. As the Ni concentration increases the diameter of the CNTs increases. On the 25% Ni:3%Cu/Al samples where maximum activity of the catalyst is observed, nanotubes with diameter of around 20-25 nm are formed and carbon in the nanotubes is aligned along the tube axis. The shape of the Ni particles present is mainly homogeneous with hollow structure. We are producing the straight, balloon and horn like carbon nanotubes which is an indication that carbon nanotubes of designed size and dimensions could be formed by the control of reaction temperature and particle size.

The Effect of K Doping on the Decomposition of CH_4. Figures 10, 11 and Table 7 present the SEM, XRD and EDX analyses of the K doped fresh and spent samples. Two

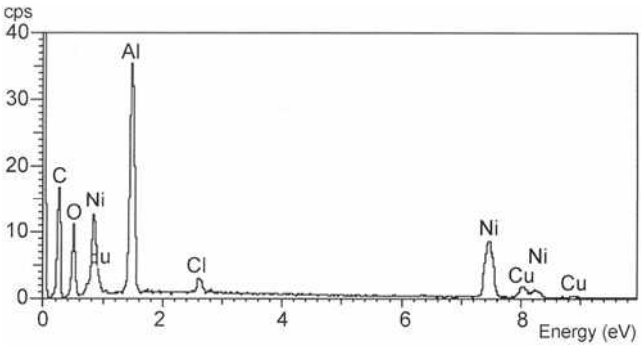

Figure 7. EDAX analysis of the 25%Ni:3%Cu after CH_4 decomposition.

Table 5. Results of EDX Analysis (contents in weight percent)

Sample		C	O	Al	Cl	Ni	Cu
25%Ni:3%Cu/Al Fresh	Mean	0.0	42.1	26.8	2.7	23.6	4.9
25%Ni:3%Cu/Al Used	Mean	48.1	22.9	11.5	0.7	13.8	3.0

Table 6. CHN analysis of 25%Ni:3%Cu/Al spent catalyst

Component Name	Retention Time (min.)	Area (.1 * uV* Sec)	Element amount	Element %
Nitrogen	0.783	1958181	0.060	2.404
Carbon	1.200	59707440	1.289	51.386
Hydrogen	3.550	23224360	0.156	6.236

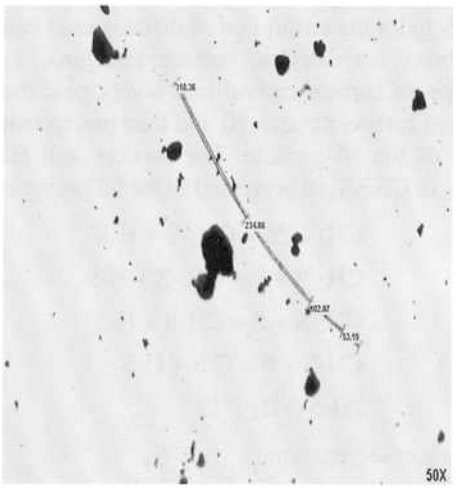

Figure 8. Presentation of the dimension of the C-nanotubes formed during CH_4 decomposition reaction.

observations are quite evident on the K doped samples; firstly the surface is very clean and no carbon formation is observed during the 10 hours run for the reaction, possibly due to formation of Ni:Cu:K surface sites which electronically modified the surface and secondly the life of the catalyst is considerably increased *i.e.* even after 30 hours continuous running the catalyst does not deactivate and the selectivity towards hydrogen production remains in the range of 18-20% (Figure 9). We propose here that the

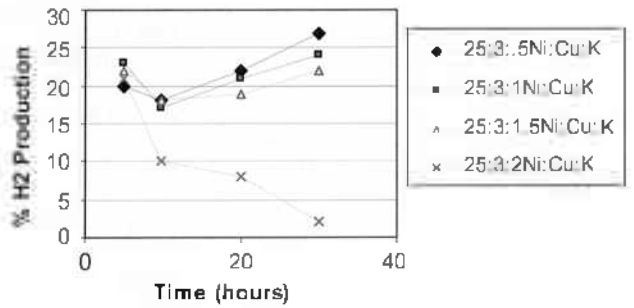

Figure 9. Effect of K doping on hydrogen production (catalyst 25%Ni:3%Cu/K_x).

potassium addition enhances the reverse reaction that is the gasification of surface carbon increases, consequently the surface is not covered by carbon. We also suggest that the addition of potassium suppresses the dissociation of methane resulting in the increase in life time of the catalyst. Figure 9 represents the % production of hydrogen *vs* K doping, which clearly indicates the effect of K addition; the catalyst remains stable upto 1.5% K doping after that the stability decreases.

Effect of Copper Addition on the Production of CNTs. On the 25% Ni/Aluimna catalyst the yield of carbon is 181 g per g of Ni. The addition of 3%Cu increases the yield of carbon formation. The highest carbon yield is on 25%Ni: 3%Cu doped samples which is 491 g per g of Ni. When the Cu concentration increases from 3%, the yield of carbon decreases. Taking the previous reports into consideration, Ni 25%/Alumina is the most effective catalyst for methane decomposition which produces 431 g carbon per g of Ni.[45,46] The addition of copper and potassium has a marked effect on our system as presented below.

1. The formation CNTs of high purity.
2. The production of pure hydrogen.
3. The enhancement of catalyst stability by K doping.

Catalytic performance of the catalyst system used in this study suggests that the methane decomposition depends on the particle size of catalyst; the increase in Ni loading may

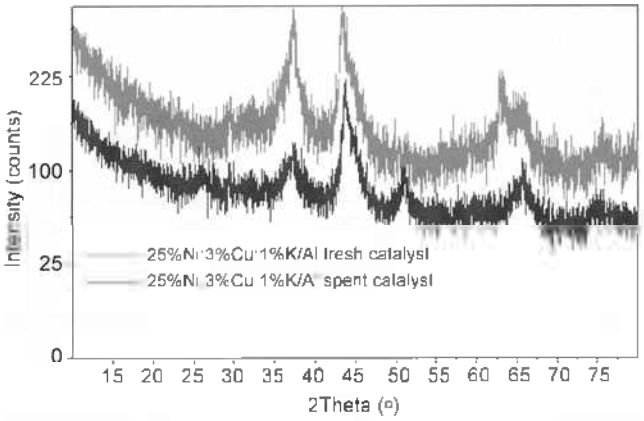

Figure 11. XRD analysis of K doped fresh and spent catalyst.

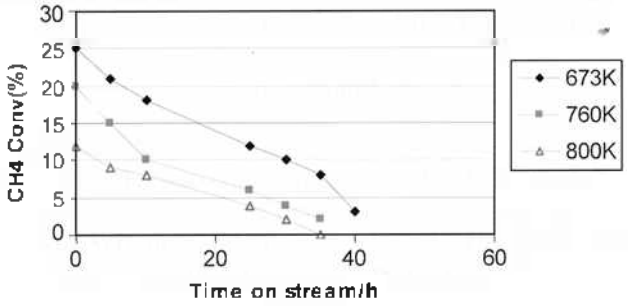

Figure 12. Kinetic curves of methane conversion in the methane decomposition over 25%Ni:3%Cu/Al_2O_3 catalyst at different temperatures.

have an effect on the decomposition of CH_4 but the major share comes from the particle size coupled with Cu doping.

We also investigated the effect of reaction temperature on the catalytic performance of 25%Ni:3%Cu/Aluimna catalyst which was the most active catalyst for methane decomposition. Figure 12 shows the kinetic curves of methane decomposition over our best catalyst. The temperature was changed from 673 K to 760 and 820 K. It is concluded from the figure that the deactivation rate of the catalyst decreases at lower temperature. Figure 13 shows the change in carbon

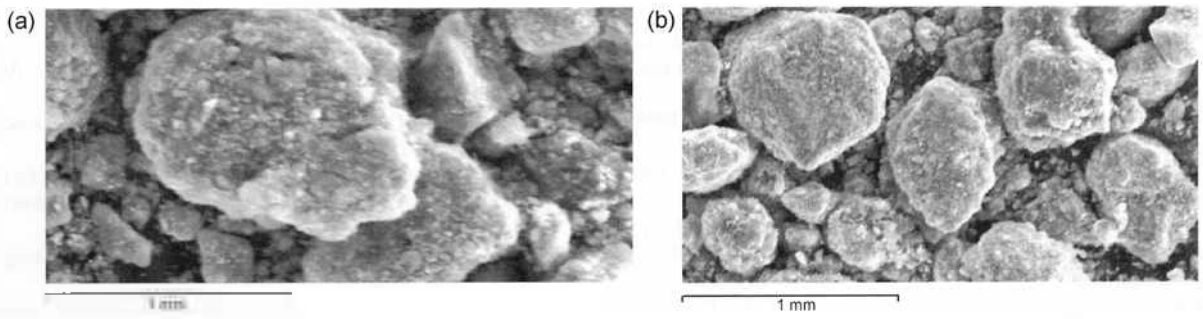

Figure 10. SEM analysis of 25%Ni:3%Cu:1%K catalyst sample; a (Fresh), b (spent).

Table 7. EDX analysis of K doped spent catalyst (contents in weight percent)

Catalyst Designation		C	O	Al	Cl	Ni	Cu	K
25%Ni:3%Cu:1%K/Al	Mean	0.0	42.1	26.8	2.7	23.6	3.9	0.91
Spent	SD	0.0	3.15	2.35	0.55	3.98	0.50	0.02

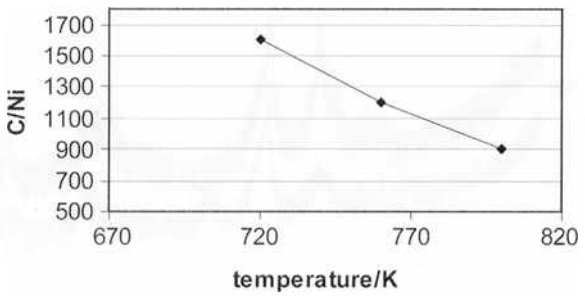

Figure 13. Change in the C/Ni as a function of reaction temperature on 25%Ni3%Cu/Al catalyst.

yield as a function of reaction temperature. As the reaction temperature becomes higher the C/Ni value decreases. This result indicates that lower temperature is needed in order to get high yield of hydrogen and carbon.

Conclusions

We conclude as follows on the basis of results described:

1. Ni(25%), Cu(3%)/Al is one of the most effective catalysts for methane decomposition. The catalyst yields carbon tubes of higher length and width with porous structure at 673 K.

2. All the copper doped catalysts produce hydrogen without the production of CO and CO_2.

3. Catalyst stability is increased substantially with the K addition.

4. The amount of carbon formed during the reaction is related to the particle size and doping with copper.

5. The yields of carbon and hydrogen decrease significantly with the increase in temperature.

6. The %age Ni dispersion increases significantly with the modified method used in this study.

Acknowledgement. The authors acknowledge the financial support of Higher Education Commission, Pakistan for this work through project No. 20-573/R & D/05/313.

References

1. Hughes, T. V.; Chamber, C. R. **1889**. *US Patent* 405480.
2. *Carbon Fibers Filaments and Composites*; Figueiredo, J. L.; Bernardo, C. A.; Baker, R. T. K., Eds.; Kluwer Academic: Dordrecht/Norwell, MA, 1990.
3. Ishihara, T.; Miyashita, H.; Iseda, H.; Takita, Y. *Chem. Lett.* **1995**, *93*, 11.
4. Otsuka, K.; Kobayashi, S.; Takenaka, S. *Appl. Catal. A* **2000**, *190*, 261.
5. Shiakhutdinov, S. K.; Avdeeva, L. B.; Goncharova, O. V.; Kochubey, D. I.; Novgorodov, B. N.; Plyasova, L. M. *Appl. Catal. A* **1995**, *126*, 125.
6. Ermakova, M. A.; Ermakov, D. Yu.; Kuvshinov, G. G.; Plyasova, L. M. *J. Catal.* **1999**, *187*, 77.
7. Takenaka, S.; Ogihara, H.; Yamanaka, I.; Otuska, K. *Appl. Catal. A* **2001**, *217*, 101.
8. Avdeeva, L. B.; Goncharova, O. V.; Kochubey, D. I.; Zaikovskii, V. I.; Plyasova, L. N.; Novgorodov, B. N.; Shaikhutdinov, Sh. K. *Appl. Catal. A* **1996**, *141*, 117.
9. Shaikhutdinov, Sh. K.; Avdeeva, L. B.; Novgorodov, B. N.; Zaikovskii, V. I.; Kochubey, D. I. *Catal. Lett.* **1997**, *47*, 35.
10. Ermakova, M. A.; Ermakov, D. Yu.; Kushinov, G. G.; Plyasova, L. M. *J. Catal.* **1999**, *187*, 77.
11. Reshetenko, T. V.; Avdeeva, L. B.; Ismagilov, Z. R.; Chuvilin, A. L.; Ushakov, V. A. *Appl. Catal. A* **2003**, *247*, 51.
12. Takenaka, S.; Kobayashi, S.; Ogihara, H.; Ostuka, K. *J. Catal.* **2003**, *217*, 79.
13. Li, J.; Lu, G.; Li, K.; Wang, W. *J. Mol. Catal. A-Chem.* **2004**, *221*, 105.
14. De Jong, K. P.; Geus, J. W. *Catal. Rev. Sci. Eng.* **2000**, *42*, 481.
15. Chambers, A.; Nemes, T.; Rodriguez, N. M.; Baker, R. T. K. *J. Phys. Chem. B* **1998**, *102*, 2251.
16. De Jong, K. P.; Geus, J. W. *Catal. Rev. Sci. Eng.* **2000**, *42*, 481.
17. Otsuka, K.; Ogihara, H.; Takenaka, S. *Carbon* **2003**, *41*, 223.
18. Reshetenko, T. V.; Avdeeva, L. B.; Ismagilov, Z. R.; Chuvilin, A. L.; Fenelonov, V. B. *Catal. Today* **2005**, *102-103*, 115.
19. Conie, L. C.; Jennifer, S.; Kenneth, J. K. *Langumir* **2002**, *18*, 1352.
20. Wang, C.; Gau, G.; Gau, S.; Tang, C.; Bi, J. *Catal. Lett.* **2005**, *101*, 241.
21. Liang, L.; Li, Y. *Chem. Lett.* **2003**, *32*, 1126.
22. Liang, Z.; Zhu, Y.; Hu, X. *J. Phys. Chem. B* **2004**, *108*, 3488.
23. Balandin, A. A. In *Advances in Catalysis*; Eley, D. D.; Frankenburg, W. G.; Komarewsky, V. I.; Weisz, P. B., Eds.; Academic Press: Orlando, FL, 1958; Vol. 10, p 96.
24. Kobozev, N. I. *Acta Physicochim* **1938**, 9, 805.
25. Dowden, D. A. *J. Chem. Soc. London* **1950**, 242.
26. Simon, D.; Bigot, F. *Surf. Sci.* **1994**, *306*, 459.
27. Lang, N. D.; Holloway, S.; Norskov, J. K. *Surf. Sci.* **1987**, *236*, 403.
28. Bengaard, H. S.; Alstrup, Ib.; Chorkendorfl, Ib.; Ullmann, S.; Rostrup-Nielsen, J. R.; Norskov, J. K. *J. Catal.* **1999**, *187*, 238.
29. Ceyer, S. T.; Yang, Q. Y.; Leem, M. B.; Beckelerie, J. D.; Johnson, A. D. *Stud. Surf. Sci. Catal.* **1987**, *36*, 51.
30. Rostrup-Nielsen, J. R. *J. Catal.* **1987**, *33*, 173.
31. Rostrup-Nielsen, J. R. *J. Catal.* **1974**, *31*, 184.
32. Rostrup-Nielsen, J. R.; Christiansen, L. *Appl. Catal. A: Gen.* **1995**, *126*, 381.
33. Rostrup-Nielsen, J. R.; Bak Hansen, J. H.; Aparicio, L. M. *J. Jpn. Petrol. Inst.* **1997**, *40*, 366.
34. Zhao, N. Q.; He, C. N.; Ding, J.; Zou, T. C.; Qiao, Z. J.; Shi, C. S.; Du, X. W.; Li, J. J.; Li, Y. D. *J. Alloy. Compd.* **2007**, *428*, 79.
35. Chai, S.; Zein, S. H. S.; Mohamed, A. R. *Chem. Phys. Lett.* **2006**, *426*, 345.
36. Inoue, M.; Asai, K.; Nagayasu, Y.; Takane, K.; Yagasaki, E. *Adv. Sci. Tech.* **2006**, *48*, 67.
37. Suelves, I.; Lazaro, M. J.; Moliner, R.; Echegoyen, Y.; Palacios, J. M. *Catal. Today* **2006**, *116*, 271.
38. Rahman, M. S.; Croiset, E.; Hudgins, R. R. *Topics in Catalysis* **2006**, *37*, 137.
39. Cullity, B. D. *Elements of X-ray Diffraction*, 2nd ed.; Addison-Wesley: Menlo Park, CA, 1978.
40. Robertson, S. D.; Menicol, B. D.; De Bass, J. H.; Kloet, S. C.; Jenkins, J. W. *J. Catal.* **1975**, *37*, 424.
41. Rostrup-Nielson, J. R. In *Steam Reforming Catalysts: An Investigation of Catalyst for Turbular Steam Rreforming of Hydrocarbons*; Teknisk Forlag A/S: Copenhagen, 1975.
42. Toebes, M. L.; Bitter, J. H.; Van Dillen, A. J.; De Jong, K. P. *Catal. Today* **2002**, *76*, 33.
43. Hernadi, K.; Konya, Z.; Siska, A.; Kiss, J.; Oszko, A.; Nagy, J. B.; Kirivsi, I. *Mater. Chem. Phys.* **2003**, *77*, 536.
44. Park, C.; Keane, M. A. *J. Catal.* **2004**, *221*, 386.
45. Ermakova, D. Yu.; Ermakov, G. G.; Plyasova, L. M. *J. Catal.* **1999**, *187*, 77.
46. De Chen; Christensen, K. O.; Fernandez, E. O.; Yu, Z.; Totdal, B.; Latorre, N.; Monzon, A.; Holmen, A. *J. Catal.* **2005**, *229*, 82.